Metabolic engineering of *Saccharomyces cerevisiae* for second-generation ethanol production from xylo-oligosaccharides and acetate

Dielle Pierotti Procópio[1], Jae Won Lee[2,3], Jonghyeok Shin[2,3], Robson Tramontina[4,5], Patrícia Felix Ávila[6], Lívia Beatriz Brenelli[7], Fabio Márcio Squina[5], André Damasio[4], Sarita Cândida Rabelo[8], Rosana Goldbeck[6], Telma Teixeira Franco[7,9], David Leak[10], Yong-Su Jin[2,3], Thiago Olitta Basso[1,*]

[1]Department of Chemical Engineering, Escola Politécnica, Universidade de São Paulo (USP), São Paulo, SP 05508-010, Brazil

[2]DOE Centre for Advanced Bioenergy and Bioproducts Innovation, University of Illinois at Urbana-Champaign, Urbana, IL 61801, USA

[3]Department of Food Science and Nutrition, University of Illinois at Urbana-Champaign (UIUC), Urbana, IL 61801, USA

[4]Department of Biochemistry and Tissue Biology, Institute of Biology, University of Campinas (UNICAMP), Campinas, SP 13083-862, Brazil

[5]Environment and Technological Processes Program, University of Sorocaba (UNISO), Sorocaba, SP 18023-000, Brazil

[6]School of Food Engineering, University of Campinas (UNICAMP), Campinas, SP 13083-862, Brazil

[7]Interdisciplinary Center of Energy Planning, University of Campinas (UNICAMP), Campinas, SP 13083-896, Brazil

[8]Departament of Bioprocesses and Biotechnology, School of Agriculture, Sao Paulo State University (UNESP), Botucatu, SP 18618-687, Brazil

[9]School of Chemical Engineering, University of Campinas (UNICAMP), Campinas, SP 13083-852, Brazil

[10]Department of Biology and Biochemistry, University of Bath, Claverton Down, Bath BA2 7AY, UK

***Correspondence:**

Thiago Olitta Basso

thiagobasso@usp.br

Highlights

- Integration of XOS pathway in an acetate-xylose-consuming *S. cerevisiae* strain;
- Intracellular fermentation of XOS, acetate and xylose improved ethanol production;
- Deletion of both *sor1*Δ and *gre3*Δ reduced xylitol production.

ABSTRACT

Simultaneous intracellular depolymerization of xylo-oligosaccharides (XOS) and acetate fermentation by engineered *Saccharomyces cerevisiae* offers an advance towards more cost-effective second-generation (2G) ethanol production. As xylan is one of the most abundant polysaccharides present in lignocellulosic residues, the transport and breakdown of XOS in an intracellular environment might bring a competitive advantage for recombinant strains in competition with contaminating microbes, which are always present in fermentation tanks; furthermore, acetic acid is a ubiquitous toxic component in lignocellulosic hydrolysates, deriving from hemicellulose and lignin breakdown. In the present work, the previously engineered *S. cerevisiae* strain, SR8A6S3, expressing NADPH-linked xylose reductase (XR), NAD^+-linked xylitol dehydrogenase (XDH) (for xylose assimilation), as well as NADH-linked acetylating acetaldehyde dehydrogenase (AADH) and acetyl-CoA synthetase (ACS) (for an NADH-dependent acetate reduction pathway), was used as the host for expressing of two β-xylosidases, *GH43-2* and *GH43-7*, and a xylodextrin transporter, *CDT-2*, from *Neurospora crassa*, yielding the engineered strain SR8A6S3-CDT_2-GH432/7. Both β-xylosidases and the transporter were introduced by replacing two endogenous genes, *GRE3* and *SOR1*, that encode aldose reductase and sorbitol (xylitol) dehydrogenase, respectively, which catalyse steps in xylitol production. Xylitol accumulation during xylose fermentation is a problem for 2G ethanol production since it reduces final ethanol yield. The engineered strain, SR8A6S3-CDT_2-$GH43_{2/7}$, produced ethanol through simultaneous co-utilization of XOS, xylose, and acetate. The mutant strain produced 60% more ethanol and 12% less xylitol than the control strain when a hemicellulosic hydrolysate was used as a mono- and oligosaccharide source. Similarly, the ethanol yield was 84% higher for the

63 engineered strain using hydrolysed xylan compared with the parental strain. The consumption of
64 XOS, xylose, and acetate expands the capabilities of *S. cerevisiae* for utilization of all of the
65 carbohydrate in lignocellulose, potentially increasing the efficiency of 2G biofuel production.
66
67 **Keywords:** *Saccharomyces cerevisiae*, xylo-oligosaccharides, acetate, xylose, lignocellulosic
68 ethanol
69
70

1. INTRODUCTION

The production of fuel ethanol from sugarcane is a major contributor to the ongoing transition from fossil to renewable fuels and chemicals (Karp et al., 2021). To increase production without a massive increase in land use requires intensification by utilising all of the fermentable carbohydrate in the sugarcane, including that present in bagasse and straw, which is composed of lignocellulose (Raj et al., 2022; Raud et al., 2019). Successfully accessing and fermenting this fraction would also open up routes to using other agricultural by-products, such as straw and forestry residues. Their procurement cost is relatively low, besides being an abundant non-food feedstock (Ko and Lee, 2018). The lignocellulosic biofuel production process requires the deconstruction of biomass into fermentable sugars and the conversion of sugars to biofuels (Li et al., 2019). Due to the complex integration of cellulose, hemicellulose, and lignin in the structure of lignocellulose, harsh pre-treatment is required to access the carbohydrate polymers for enzymatic hydrolysis and fermentation, which can result in the production of by-products such as furans, organic acids, phenols and inorganic salts which can inhibit microbial metabolism (Ask et al., 2013; Kłosowski and Mikulski, 2021; Tramontina et al., 2020).

Pre-treatment aims to reduce the crystallinity of cellulose, and partially degrade hemicellulose and lignin to increase the susceptibility of the biomass to enzymatic cocktails, which in turn are necessary to breakdown polysaccharides into fermentable monomeric sugars (Kłosowski and Mikulski, 2021; Sarkar et al., 2012; Sharma et al., 2020). However, during the degradation of hemicellulose and lignin, acetic acid production is unavoidable as hemicellulose and lignin are acetylated (Chen et al., 2019; Klinke et al., 2004). This is toxic to yeast metabolism, reducing sugar fermentation efficiency and biofuel yield (Almeida et al., 2007; Kłosowski and Mikulski, 2021; Salas-Navarrete et al., 2022). Weak organic acids, such as acetic acid, can diffuse

94 undissociated through the cell membrane and dissociate inside the cell, releasing protons and
95 lowering the internal pH value (Bellissimi et al., 2009; Kłosowski and Mikulski, 2021). To
96 overcome the inhibitory effect of acetic acid, Zhang et al., (2016) introduced an optimized route
97 for acetate reduction, through the expression of three copies of codon-optimized acetaldehyde
98 dehydrogenase - *adhE* (CO_*adhE*) from *Escherichia coli,* and three copies of a mutated acetyl-
99 CoA synthetase - *ACS* (*ACS*Opt*) from *Salmonellas enterica* into a xylose-fermenting *S.*
100 *cerevisiae* strain, which produces recombinant NADPH-linked xylose reductase (XR) and NAD^+-
101 linked xylitol dehydrogenase (XDH), yielding strain SR8A6S3. This strategy enabled efficient
102 xylose fermentation with 29.7% higher ethanol yield and 70.7% lower by-product (xylitol and
103 glycerol) production when cultivated in YP medium supplemented with 20 g L^{-1} glucose, 80 g L^{-1}
104 xylose, and 8 g L^{-1} acetate under strict anaerobic (anoxic) conditions. The reduction of acetate to
105 ethanol serves as an electron sink to alleviate the redox cofactor imbalance resulting from *XR* and
106 *XDH* activities (Wei et al., 2013), with NAD^+ generated from the reductive metabolism of acetate
107 being available for XDH activity, thus reducing the production of xylitol and glycerol. Thus, this
108 strategy can provide multiple benefits for the ethanol industry (Zhang et al., 2016).

109 Although SR8A6S3 can tolerate acetic acid present in lignocellulosic hydrolysates, many
110 other inhibitory compounds are also released during the pre-treatment steps (Kłosowski and
111 Mikulski, 2021). While less severe pre-treatment could be considered for achieving a lower
112 concentration of inhibitors, a large amount of cellulase and hemicellulase enzyme cocktails would
113 still be required for converting cellulose and hemicellulose into monomeric sugars, posing
114 unsolved economic and logistical challenges for the industry (Adsul et al., 2020; Chundawat et al.,
115 2011; Himmel et al., 2007; Li et al., 2015). One possible strategy to achieve economic 2G ethanol
116 is to use *S. cerevisiae* strains genetically modified to transport and intracellularly utilize cellulose

and hemicellulose-derived oligosaccharides. Such a microorganism might have a competitive advantage over other microorganisms, such as contaminating bacteria and wild *Saccharomyces* and non-*Saccharomyces* species, which are not able to metabolize oligosaccharides, as well as requiring lower amounts of hemi/cellulolytic enzymes, which should translate into a cheaper process (Procópio et al., 2022).

In previous work, Li and co-authors (Li et al., 2015) expanded xylose utilization by an engineered *S. cerevisiae* strain, to incorporate the transport and intracellular hydrolysis of XOS to xylose monomers through the expression of two β-xylosidases, *GH43-2*, and *GH23-7*, and a XOS-transporter, *CDT-2*, from *N. crassa* in a xylose-utilizing host strain. Both glycoside hydrolases (GH) catalyse the hydrolysis of 1,4-β-D-xylosidic linkages in xylan (Mewis et al., 2016). The new strain could produce more than 30 g L^{-1} of ethanol in 72h of cultivation in an optimized minimum medium (oMM) supplemented with 4% xylose and 3% XOS under anaerobic conditions.

In this work, we used the SR8A6S3 strain as a platform for the construction of a yeast strain able to ferment XOS, xylose, and acetate into ethanol (**Fig. 1**). Genes encoding the XOS-transporter (c*dt-2*) and both of the β-xylosidases (*gh43-2* and *gh43-7*) from *N. crassa* were integrated into the SR8A6S3 genome (highlighted in the yellow area in **Fig. 1**). First, a high expression cassette for *cdt-2* expression was integrated into the sorbitol (xylitol) dehydrogenase *locus*, encoded by gene *sor1* gene, through the locus-specific CAS-9-based integration system (Stovicek et al., 2015). Then, both *gh43-2* and *gh43-7* under the control of the *GAP* and *CCW12* promoters, respectively, were integrated into the aldose reductase encoded by *gre3* gene using the same locus-specific integration tool. The resulting disruption of *GRE3* and *SOR1* was designed to mitigate xylitol production and divert more carbon towards ethanol production in the recombinant strain (Jeong et al., 2020; Toivari et al., 2004; Träff et al., 2001). Conversion of hemicellulosic-

140 derived residues into industrial products, such as 2G ethanol, can contribute to the progress of
141 global warming mitigation (Sun et al., 2021).
142

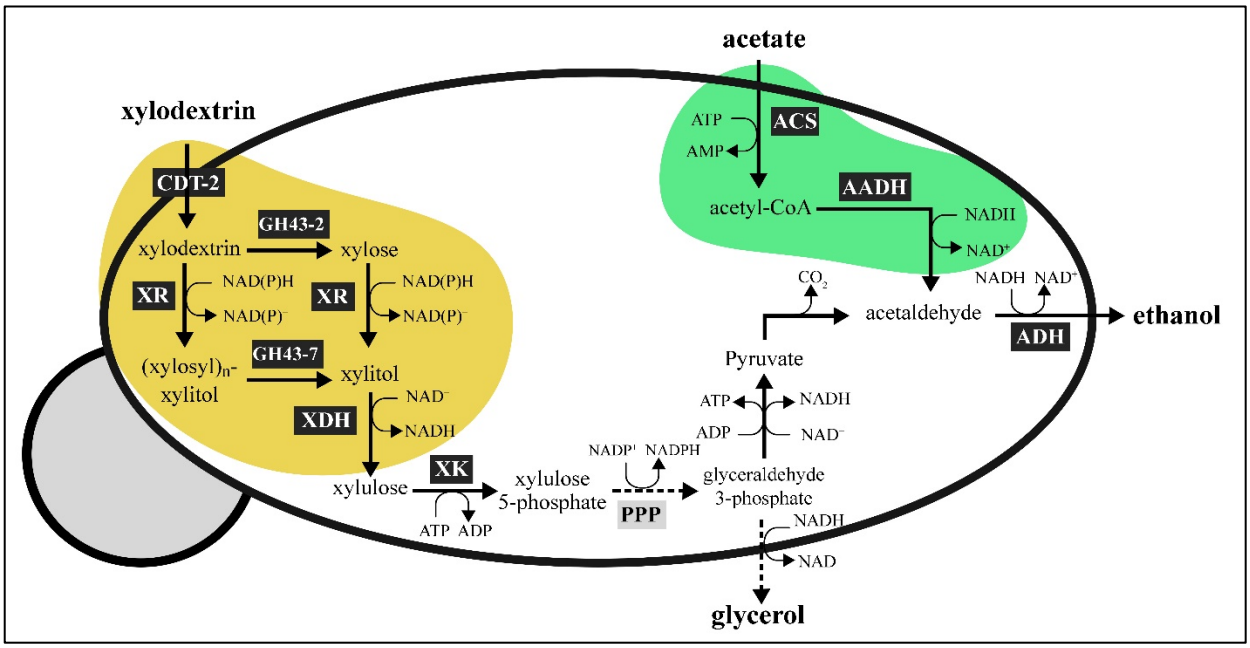

143

144 **Fig. 1**. Expected routes of XOS metabolism after expression of the XOS-transporter (*CTD-2*) and
145 beta-xylosidases (*GH43-2* and *GH43-7*) from *N. crassa* in SR8A6S3, including xylose metabolism
146 by xylose reductase (XR) and xylitol dehydrogenase (XDH) from *S. stipitis*. The surplus NADH
147 produced during xylose fermentation can be exploited to detoxify acetate, reducing it to ethanol
148 through the exogenous acetate reduction pathway, involving conversion of acetate into acetyl-CoA
149 by acetyl CoA synthetase (ACS), production of acetaldehyde from the acetyl-CoA by the
150 acetylating acetaldehyde dehydrogenase (AADH) and ethanol production from acetaldehyde by
151 the action of alcohol dehydrogenase (ADH).
152

153 ## 2. MATERIALS AND METHODS

154 ### 2.1. Strains and media

155 *E. coli* strain DH5α was used for the construction and propagation of plasmids. *E. coli* was
156 cultured in Lysogeny Broth (LB) medium (5 g L^{-1} yeast extract, 10 g L^{-1} tryptone, and 10 g L^{-1}
157 NaCl) at 37 °C and 100 μ/mL ampicillin (LBA) was added for selection when required. All
158 engineered *S. cerevisiae* strains used and constructed in this work are summarized in **Table 1**.
159 Yeast strains transformed with plasmids containing antibiotics were propagated on YPD plates
160 supplemented with the plasmid corresponding antibiotics, such as clonNAT (100 μg mL^{-1}),
161 geneticin G418 (200 μg mL^{-1}), hygromycin B (200 μg mL^{-1}). The SR8A6S3-CDT_2 strain was
162 generated by integrating the CDT-2 transporter overexpressing gene cassette into the *SOR1* locus
163 of the SR8A6S3 genome. To construct an XOS-utilizing strain the $_P$GAP–GH43-7-$_T$CYC-
164 $_P$CCW12-GH43-2-$_T$CYC1 was integrated at the *GRE3* locus of SR8A6S3-CDT_2, yielding strain
165 SR8A6S3-CDT_2-$GH43_{2/7}$.
166
167 **Table 1**. The yeast strains used in this study.

Strain	Description	Reference
SR8	Efficient xylose-consuming strain (evolved strain of D452-2 *leu2::LEU*_[RS305_TDH3$_p$_XYL1_TDH3$_T$ *ura3::URA3*_pRS-X123 *his::HIS*_pRS3-X123, and *ald6::AUR1-C* pAUR_d_ALD6)	(Kim et al., 2013)
SR8A6S3	SR8 expressing three copies of COadhE overexpression cassette and three copies of mutant *Salmonella* ACS gene overexpression cassette	(Zhang et al., 2016)
SR8-XD	SR8 expressing one copy of CDT2, GH43-2, and GH43-7 overexpression cassette	(Sun, 2020)
SR8A6S3-CDT_2	SR8A6S3 expressing one copy of CDT2 overexpression cassette	This work

SR8A6S3-CDT$_2$-GH43$_{2/7}$	SR8A6S3-CDT$_2$ expressing one copy of *GH43-2* and *GH43-7* overexpression cassette	This work

168

169 **2.2. Plasmids and strain construction**

170 All plasmids and primers in this work are summarized in **Tables 2** and **S1**, respectively.
171 The guide RNA (gRNA) plasmids (**Table 3**) gRNA-sor-K and gRNA-gre-K were amplified from
172 Cas9-NAT by using primers pair DPO_089 and DPO-090, DPO_087 and DPO_088 carrying a 20
173 bp PAM sequence for *SOR1* and *GRE3 loci*, respectively. The gRNAs were predicted by the
174 website: https://www.atum.bio/eCommerce/cas9/input. All gRNA sequences are listed in **Table 3.**

175 For genomic integration of *CDT-2* through CRISPR-Cas9-based integration in the *SOR1*
176 gene site of SR8A6S3, CDT-2 donor DNA was amplified from plasmid pRS426-CDT2 using a
177 primer pair DPO_081 and DPO_082. Transformants with *CDT-2* integration were identified by
178 PCR using primers DPO_083 and DPO_084 and the resulting strain was designated as the
179 SR8A6S3-CDT$_2$ (**Table 1**). The PCR reaction was performed using 1.25 µL forward primer, 1.25
180 µL reverse primer, DNA sample 1 µL, Phusion high-fidelity DNA polymerase master mix with
181 HF buffer (New England BioLabs) 12.5 µL, and nuclease-free water 9 µL.

182 To generate transformant strains expressing the GH43-7_GH32-2 gene cassette, the
183 sequence *GH43-7-$_T$CYC-$_P$CCW12-GH43-2* was amplified from the genomic DNA of the XOS-
184 consuming strain, SR8-XD (**Table S1**). Firstly, SR8-XD genomic DNA was prepared with the
185 Rapid Yeast Genomic DNA Extraction Kit (Bio Basic Inc., Markham Ontario, CA) and quantified
186 by NanoDrop ND-1000. Primer pairs of DPO_059 and DPO_063 were used to amplify the *GH43-*
187 *7-$_T$CYC-$_P$CCW12-GH43-2* gene sequence. The PCR product *GH43-7-$_T$CYC-$_P$CCW12-GH43-2*
188 was amplified again using a primer pair of DPO_062 and DPO_074 which has homology with
189 plasmid p426GPD. Similarly, the plasmid p426GPD was amplified using a primer pair of

DPO_064 and DPO_065. PCR was performed using 1.25 µL forward primer, 1.25 µL reverse primer, DNA sample 1 µL, Phusion high-fidelity DNA polymerase master mix with HF buffer (New England BioLabs) 12.5 µL, and nuclease-free water 9 µL. Both the linear sequences were transformed into competent *E. coli* DH5α to form the plasmid p426-GH43$_{2/7}$ (Kostylev et al., 2015) (**Table S1**). *$_P$TDH3-GH43-7-$_T$CYC-$_P$CCW12-GH43-2-$_T$CYC1* donor DNA was amplified from plasmid p426-GH43$_{2/7}$ using a primer pair DPO_057 and DPO_058.

Table 2. Plasmids used in this study.

Plasmids	Description	Reference
pRS42K	pRS42K, Kanamycin resistance gene	(Liu et al., 2016)
p426GPD	pRS426-*pTDH3-tCYC1*	Addgene (#14156)
Cas9-NAT	P414-*pTEF1-Cas9-tCYC1-NAT1*	Addgene (#64329)
p426-CDT2	pRS425-*pPGK1-CDT2-tCYC1*	(Kim et al., 2014)
gRNA-sor-K	pRS42K carrying *SOR1* disruption gRNA cassette	This work
gRNA-gre-K	pRS42K carrying *GRE3* disruption gRNA cassette	This work
p426-GH43$_{2/7}$	pRS426-*pTDH3-GH43-7-$_T$CYC- $_P$CCW12-GH43-2 tCYC1*	This work

Table 3. gRNA used in this study.

gRNA (5'- 3')	Insertion locus	Plasmid	Reference
TGTGTCGAACCCTTATCAGT	*SOR1*	gRNA-sor-K	This study
TCCTCAATCATTCATTGAGA	*GRE3*	gRNA-gre-K	This study

Transformation of yeast cells was carried out by the polyethylene glycol (PEG)-LiAc method (Gietz et al., 1995). One microgram of DNA was used for Cas9 or gRNA plasmid

transformation, 1.5 µg of donor DNA was used for homologous recombination. Correct integration was confirmed by PCR using primers DPO_069 and DPO_070. The recombinant strain was designated as SR8A6S3-CDT$_2$-GH43$_{2/7}$ (**Table 1**).

3.3. Enzyme activity assay and protein quantification

SR8A6S3-CDT$_2$-GH34$_{2/7}$ and SR8A6S3 were grown in 22 mL of yeast extract-peptone (YP) medium (10 g L^{-1} yeast extract, 20 g L^{-1} peptone) containing 2% glucose, 8% xylose, and 0.8% acetate (YPDXA) until late log phase before harvesting by centrifugation. Yeast cell pellets, 0.24 g for SR8A6S3-CDT$_2$-GH34$_{2/7}$ and 0.21 g for SR8A6S3, were resuspended in buffer containing 0.1 mM $CaCl_2$, 50 mM Tris-HCl, 100 mM NaCl, 1 mM DTT, 0.1% Triton X, pH 7.4, 0.1mM PMSF (Thermo Fisher Scientific). The cells were disrupted by agitation using 1 g glass beads and ultrasonic bath at 40% amplitude for 5 minutes on ice. The resulting lysates were centrifugated at 14,000×g for 20 min at 4 °C, and the clarified supernatant was used as an enzyme source for β-xylosidase assays.

β-xylosidase activity was measured according to Tramontina et al. (2016). Briefly, 30 µL of the clarified supernatant and 50 µL of 5 mM ρ-Nitrophenyl-β-D-xylopyranoside (pNPX) solution were added to 20 µL of reaction buffer (250 mM MES, and 5 mM $CaCl_2$, pH 7), which was then incubated at 30 °C for 60 min for the enzyme reaction. The reaction was stopped by adding 100 µL of 2 M Na_2CO_3 and the amount of ρ-Nitrophenol produced was estimated spectrophotometrically at a wavelength of 405 nm and the absorbance converted to concentration using a standard curve. One unit of enzyme activity was defined as the amount of enzyme catalysing the hydrolysis of 1 µmol pNPX per minute in 1 mL of yeast intracellular lysate (µmol mL^{-1} min^{-1}) "U mL^{-1}", or per mg of total lysate protein (µmol mg^{-1} min^{-1}) "U mg^{-1}", or per gram

226 of cells (μmol g_{CDW}^{-1} min^{-1}) under the described assay conditions. The protein concentrations in
227 each sample were determined using the Bradford dye method (Bradford, 1976).
228
229 **3.4. Fermentation and analytical methods**
230 Anaerobic batch fermentation experiments were performed in 100 mL serum bottles with
231 30 mL fermentation media. Serum bottles were sealed with a butyl rubber stopper and then flushed
232 with nitrogen gas, which had been passed through a heated, reduced copper column to remove
233 traces of oxygen. Micro-aerobic batch fermentation experiments were performed in a 125 mL
234 Erlenmeyer flask with 30 mL of fermentation media. Both anaerobic and micro-aerobic cultures
235 were incubated in a rotary shaker at 100 rpm at 30 °C.
236 For all cultivations, yeasts were pre-grown in yeast extract-peptone (YP) medium (10 g L^{-1}
237 yeast extract, 20 g L^{-1} peptone) supplemented with 20 g L^{-1} glucose, harvested by centrifugation
238 at 3,134 ×g, at 4°C for 5 min, and washed three times with sterile distilled water. Washed yeast
239 cells were inoculated in serum bottles or Erlenmeyer flasks containing either: YP supplemented
240 with a mixture of glucose, xylose, and acetate (YPDXA); hemicellulosic hydrolysate (YPH);
241 hemicellulosic hydrolysate, xylose and acetate (YPXAH); hydrolysed xylan (YPXy); hydrolysed
242 xylan and acetate (YPAXy). Initial cell concentration varied according to the cultivation, OD_{600}
243 was 1 or 10. Xylan hydrolysis was carried out according to (Ávila et al., 2020). The hemicellulosic
244 hydrolysate from sugarcane straw was obtained by a two-stage procedure: mild acetylation at 60
245 °C, 30 min, 0.8% (w w^{-1}) of NaOH and 10% (w w^{-1}) of solids followed by hydrothermal pre-
246 treatment at 190 °C, 20 min, 10% (w w^{-1}) of solids. The hemicellulosic hydrolysate obtained after
247 the second step was enzymatically treated with a GH11 from *Neocallimastix patriciarum*
248 (Megazyme® Ireland) as detailed described elsewhere (Brenelli et al., 2020). Afterwards, the

hemicellulosic hydrolysate rich in XOS was concentrated approximately 5-fold in a rotary vacuum evaporator. **Table 4** shows the chemical composition of the XOS-rich hemicellulosic hydrolysate.

Table 4. Chemical composition of the XOS-rich hemicellulosic hydrolysate after treatment with a endoxylanase GH11 and concentration.

Component	AA	FA	FT	AR	AOS	GOS	Xyl	HMF	FL	XOS
Concentration (g L^{-1})	0.77	2.51	6.40	3.93	2.45	6.91	2.74	0.07	0.01	49.67

Legend: AA - acetic acid, FA - formic acid, FT – total phenolics, AR - arabinose, AOS - arabino-oligosaccharides, GOS - gluco-oligosaccharides, Xyl - xylose, HMF - hydroxymethylfurfural, FL - furfural, XOS - total xylo-oligosaccharides.

Samples were taken using syringe and needle from serum bottles or manual single-channel pipette (Gilson, USA) from Erlenmeyer flasks at appropriate intervals to measure cell growth and metabolites concentrations. Cell growth was monitored as the optical density at 600 nm (OD600) measured using a UV-visible Spectrophotometer (Biomate 5). The samples were centrifuged at 14,000×g for 10 min and supernatants diluted appropriately for the determination of glucose, xylose, xylitol, glycerol, succinate, acetic acid, and ethanol by high-performance liquid chromatography (HPLC, Agilent Technologies 1200 Series) equipped with a refractive index detector (RID). Chromatography was done on a Rezex ROA-Organic Acid H+ (8%) column (Phenomenex Inc., Torrance, CA) maintained at 60 °C, with 0.005 N H_2SO_4 as eluent at a flow rate of 0.6 mL min^{-1}. Analyte concentrations were determined by using the RID detector.

2.3.1. Xylo-oligosaccharide quantification

The enzymatic products were analysed by high-performance anion-exchange chromatography with pulsed amperometry detection (HPAEC–PAD) to detect xylose and XOS produced by the xylanase enzymes. Separation was performed using a Dionex ICS-3000 instrument (Thermo Fisher Scientific, Sunnyvale, CA, USA) with a CarboPac PA100 column (4×250 mm) and CarboPac PA100 guard column (4×50 mm), eluted with a linear gradient of A (NaOH 500 mM) and B (NaOAc 500 mM, NaOH 80 mM). The gradient program was 15 % of A and 2 % of B for 0–10 min, followed by 15–50 % of A and 2–20 % of B from 10–20 min, with a flow rate of 1.0 mL min^{-1}. The integrated peak areas were converted to concentrations based on standards (×1 to×6).

3. RESULTS AND DISCUSSION

3.1. Cas9- based integration of CDT-2 expression cassette into the *SOR1* locus

Although xylitol has a variety of uses in the food, cosmetic, nutraceutical, and pharmaceutical industries (Queiroz et al., 2022), this metabolite may face competition from an available carbon source, reducing the efficiency of ethanol production. *S. cerevisiae* strains possess genes encoding enzymes capable of xylose reduction, such as *GRE3*, *GCY1*, *YPR1*, *YDL124W*, *YJR096W*, and xylitol oxidation such as *XYL2*, *SOR1*, *SOR2, XDH1*, which can result in xylitol formation during xylose fermentation (Wenger et al., 2010). To reduce xylitol production and divert the carbon to ethanol production, *SOR1* was replaced by a *CDT-2* expression cassette in the genomic DNA of strain SR8A6S3, yielding SR8A6S3-CDT_2. The required integration of the *CDT-2* cassette was confirmed by PCR analysis. Colony PCR was performed directly from 27 colonies of the positive-control plate (**Fig. S1**). Once the desired integration was confirmed, both SR8A6S3-

291 CDT_2 and SR8A6S3 strains were compared in anaerobic and micro-aerobic batch cultures (**Fig.**
292 **2.A**, **2.B** and **3**) in YPDXA containing 20 g L^{-1} glucose, 80 g L^{-1} xylose, and 8 g L^{-1} acetate, with
293 an initial OD600 of 1.

294 Deletion of *sor1* led to a reduced rate of xylose and acetate consumption under both
295 anaerobic and micro-aerobic conditions (**Fig. 2.A**, **2.B,** and **3**). Under anaerobic batch cultivation,
296 75% of the initial xylose was consumed by the SR8A6S3 strain, while SR8A6S3-CDT_2 was only
297 able to consume 53% of the original concentration within 72 h (**Fig. S2.A**). The xylose
298 consumption rate of SR8A6S3 was also higher after 24h of anaerobic cultivation in comparison to
299 SR8A6S3-CDT_2 (**Table 5**).

300 Concerning acetate metabolism, the control strain consumed 71% of the initial acetate in
301 the medium, while SR8A6S3-CDT_2 consumed only 43% in 72 h of cultivation (**Fig. 2.A**, **2.B,** and
302 **S2.E**). For glucose metabolism, no difference was observed between the two strains (**Fig. 2**).
303 However, despite the greater consumption of xylose and acetate by the control strain (83.08 ± 1.46
304 versus 70.58 ± 2.91 g L^{-1}), SR8A6S3-CDT_2 had a slightly higher ethanol yield (**Table 5**) and
305 produced 66% less xylitol and 12% less glycerol as a by-product (**Fig. S2**). We observed that
306 glycerol was primarily coming from glucose for both cultivations. Great amount of total glycerol
307 was produced at 24 h of cultivation, 66% for SR8A6S3 and 60% for SR8A6S3-CDT_2. Considering
308 these results, it is possible to conclude that in the control strain cultivation, the carbon source was
309 channelled towards metabolites whose pathways allowed the balance of redox cofactors, such as
310 xylitol and glycerol. Thereby, *sor1* is responsible for a significant amount of xylitol production
311 but *sor1*Δ primarily slows down xylose metabolism. Whereas *sor1*Δ enabled the engineered strain
312 to drive more carbon toward the desired product (ethanol). Presumably, this is because the NADH
313 / NAD^+ balance has changed while the ethanol yield has increased marginally via the pyruvate

314 decarboxylase (PDC) route as, relative to xylose, acetate metabolism is proportionally lower when
315 the two strains are compared.

316 Some metabolites were measured to compare the fermentation profiles of SR8A6S3-CDT$_2$
317 and SR8A6S3 (**Fig. S2**). Elimination of xylitol production through *sor1*Δ increases the availability
318 of intracellular NADH, which enabled the recombinant cell to produce more ethanol per gram of
319 consumed sugar (ethanol yield). Deletion of the *sor1* gene activity does not eliminate xylitol
320 production since other genes encode enzymes capable of xylose reduction or xylitol oxidation,
321 resulting in xylitol production. However, under strict anaerobic cultivation, the xylitol amount was
322 reduced from 1.9 g L^{-1} to 0.69 g L^{-1} comparing parental and recombinant strains, respectively (**Fig.**
323 **S2.C**). In principle, NAD$^+$ should be available to drive the xylitol to xylulose reaction.
324

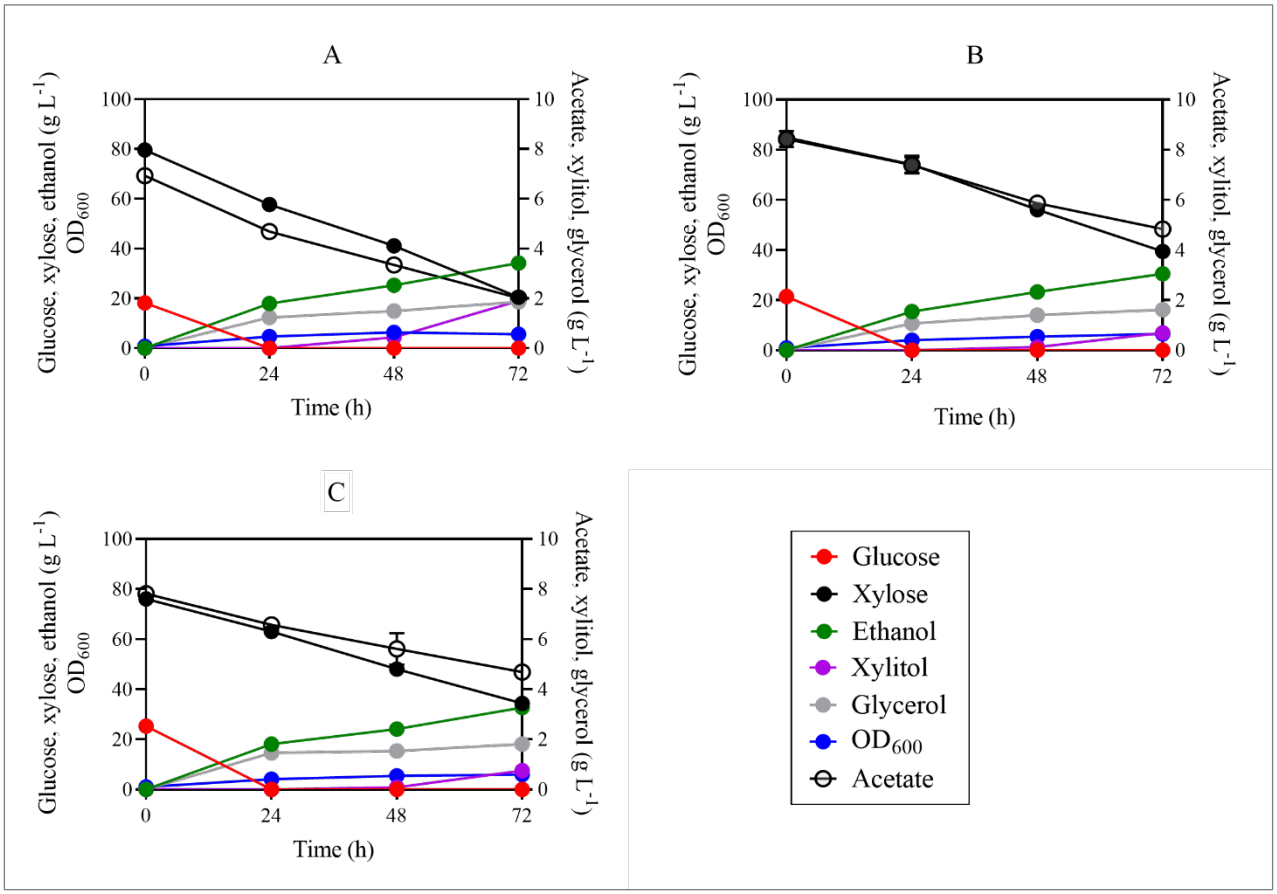

325

Fig. 2. Fermentation profiles of SR8A6S3 (A), SR8A6S3-CDT_2 (B), and SR8A6S3-CDT_2-$GH43_{2/7}$ (C) when fermenting YP supplemented with 20 g L^{-1} glucose, 80 g L^{-1} xylose, and 8 g L^{-1} acetate) under strictly anaerobic conditions. Data are presented as mean values and standard deviations of three independent biological replicates.

Under strict anaerobic conditions, ethanol is the most important primary metabolite produced in terms of re-oxidation of excess NADH and redox balancing, followed by the production of glycerol (Jain et al., 2011), which is important to support xylulose production from xylitol. When oxygen is available in the flask, redox balancing of NADH / NAD^+ can also occur through the electron transport chain, which should result in less xylitol accumulation in the medium. We corroborated this hypothesis during batch cultivations under micro-aerobic conditions, where lower xylitol production was observed for both strains (**Fig. 3** and **S3.C**). Micro-aerobic batch fermentations were performed in complex YP media supplemented with 20 g L^{-1} glucose, 80 g L^{-1} xylose, and 8 g L^{-1} acetate with an initial OD_{600} of 1 (**Fig. 3** and **S3**).

Under micro-aerobic conditions the ethanol yields of SR8A6S3-CDT_2 and SR8A6S3 were 0.39 $g_{Ethanol}$ $(g_{consumed\ sugars})^{-1}$ and 0.37 $g_{Ethanol}$ $(g_{consumed\ sugars})^{-1}$, respectively. As expected, xylitol yield was lower in SR8A6S3-CDT_2 than in SR8A6S3, 0.004 $g_{Xylitol}$ $(g_{consumed\ xylose})^{-1}$ against 0.009 $g_{Xylitol}$ $(g_{consumed\ xylose})^{-1}$, respectively. Until 48 h of cultivation, SR8A6S3-CDT_2 consumed 79% of the initial concentration of acetate, whereas SR8A6S3 consumed slightly lower amounts, 73%. After 48 h, both strains star oxidising the ethanol back to acetate (**Fig. 3**).

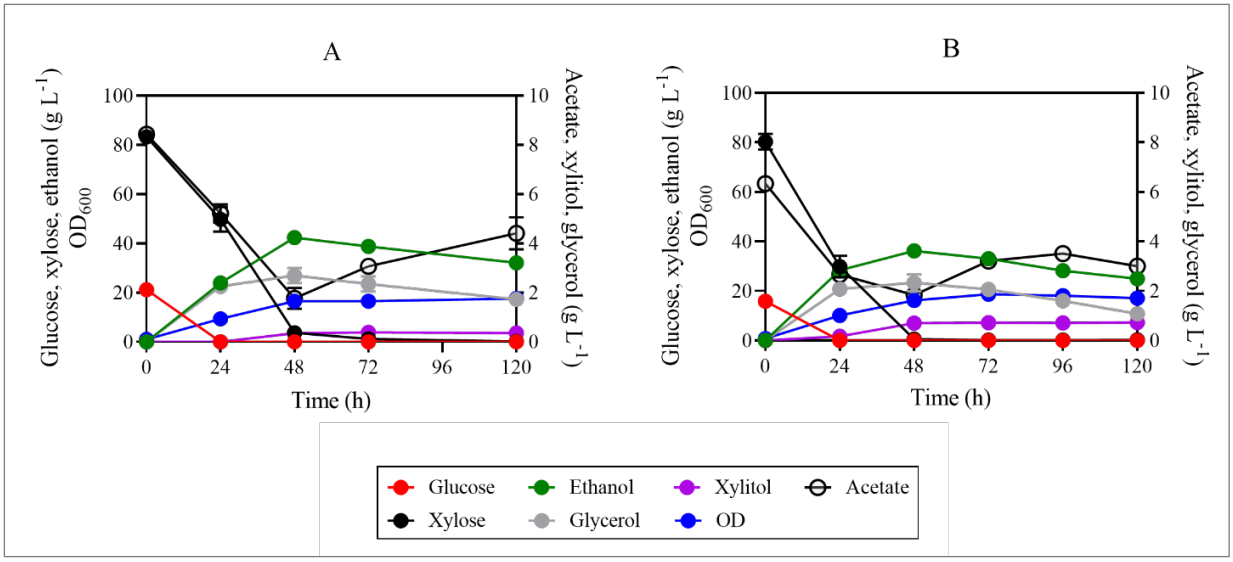

Fig. 3. Fermentation profiles of the SR8A6S3-CDT$_2$ (A), SR8A6S3 (B) when fermenting 20 g L^{-1} glucose, 80 g L^{-1} xylose, and 8 g L^{-1} acetate under micro-aerobic conditions. Data are presented as mean values and standard deviations of three independent biological replicates.

3.2. Cas9- based integration of a GH43-2_GH43-7 expression cassette into the *GRE3 locus*

GRE3 is an important xylose-reducing enzyme expressed by *S. cerevisiae* strains, the deletion of which decreases xylitol formation (Träff et al., 2001). Therefore, to further decrease carbon diverted to xylitol formation, a cassette for *GH43-2* and *GH43-7* high expression was integrated into the *gre3* locus of SR8A6S3-CDT$_2$ using a CAS-9-based system (Stovicek et al., 2015), yielding the SR8A6S3-CDT$_2$-GH43$_{2/7}$ strain. The desired integration of the GH43$_{2/7}$ sequence cassette into SR8A6S3-CDT$_2$-GH43$_{2/7}$ was confirmed by colony PCR performed on 7 colonies from the positive-control plate (**Fig. S4**). Once correct integration was confirmed, a positive transformant was then evaluated for growth in xylose and acetate, hydrolysed xylan, and hemicellulosic hydrolysate.

Thereby, to investigate the latest engineered strain, a YP-based medium was used to cultivate SR8A6S3-CDT$_2$-GH43$_{2/7}$ and measure xylose and acetate fermentation performance

compared with SR8A6S3-CDT_2 and their parental strain, SR8A6S3. Anaerobic batch cultivation was carried out for xylose and acetate consumption evaluation, and ethanol and xylitol production in high sugar content media (20 g L^{-1} glucose, 80 g L^{-1} xylose, and 8 g L^{-1} acetate) with an initial OD600 of 1 (**Fig. 2** and **S5**).

In the first 24 h of cultivation, SR8A6S3-CDT_2-$GH43_{2/7}$ had an increased xylose consumption profile, compared with the SR8A6S3-CDT_2 strain. The latest engineered strain consumed 13.65 ± 0.53 g L^{-1} of xylose, which represents 18% of the initial xylose concentration, and the immediate parent consumed 10.73 ± 0.53 g L^{-1} (15% of the initial xylose concentration). During the same period, the acetate consumption profile was slightly higher for SR8A6S3-CDT_2-$GH34_{2/7}$ than SR8A6S3-CDT_2, 17% against 15% of the initial acetate concentration, respectively (**Fig. 2B** and **2C**). Following a similar line of analysis, the glycerol production profile, within the first 24 h, was higher for SR8A6S3-CDT_2-$GH34_{2/7}$ than for SR8A6S3-CDT_2 strain. The first produced 1.47 ± 0.04 g L^{-1} and the second one achieved 0.98 ± 0.13 g L^{-1} of glycerol. Conversely, within 24 and 72 h of cultivation, SR8A6S3-CDT_2-$GH43_{2/7}$ consumed lesser amounts of xylose and acetate than its immediate parent strain, 28.84 ± 0.66 g L^{-1} against 34.61 ± 3.45 g L^{-1} for xylose and 1.81 ± 0.14 g L^{-1} against 2.38 ± 0.14 g L^{-1} for acetate, respectively; as well as produced lesser amounts of glycerol, 0.34 ± 0.04 g L^{-1} against 0.66 ± 0.12 g L^{-1}, respectively for SR8A6S3-CDT_2-$GH43_{2/7}$ and SR8A6S3-CDT_2 (**Fig. 2B** and **2C**). The change in the profile of xylose, acetate, and glycerol for both strains in the first 24 h of cultivation and after this time, presumably is because of the change in the balance of NADH / NAD^+. Deletion of *gre3* and increased production of glycerol (within 24 h of cultivation) might result in higher availability of the cofactors required for xylose metabolism (**Fig. S6**), which reflected better xylose consumption profile for SR8A6S3-CDT_2-$GH43_{2/7}$ in the first 24 h of cultivation. After the depletion of glucose, the glycerol

387 production profile decreased for both strains (**Fig. 2B** and **2C**) but *gre3*Δ slows down xylose
388 metabolism.

389 Instead, compared with SR8A6S3 (**Fig. 2A** and **2B**), the latest engineered strain had
390 impaired xylose and acetate consumption profiles during all times of cultivation. Within the first
391 24 h of cultivation, SR8A6S3 consumed 22.53 ± 1.24 g L^{-1} of xylose, which represents 28% of the
392 initial concentration, and 2.28 ± 0.10 g L^{-1} of acetate. The doubly engineered strain after 72h
393 consumed only 56% and 40% of the initial concentration of xylose and acetate, respectively,
394 although, intriguingly, rate of xylose consumption was marginally higher than the parent strains
395 after 24h. However, SR8A6S3-CDT_2-$GH43_{2/7}$ had a slightly higher ethanol yield compared to both
396 SR8A6S3-CDT_2 and SR8A6S3 (**Table 5**). Therefore, although xylitol production after 72h was
397 similar for SR8A6S3-CDT_2-$GH43_{2/7}$ and SR8A6S3-CDT_2 deletion of both *sor1*Δ and *gre3*Δ,
398 which should increase the availability of intracellular NADH and $NADP^+$, enabled cells to produce
399 more ethanol per gram of consumed sugar (ethanol yield) than the *sor1*Δ single deletion (**Fig. S6**).
400 Moreover, the biomass production profile, which was analysed by measurement of OD_{600}, of
401 SR8A6S3-CDT_2-$GH43_{2/7}$ and SR8A6S3-CDT_2 was similar until 24 h but was lower for the
402 reference strain. The double-engineered strain and its immediate parent presented an increase in
403 biomass content of 2.95 ± 0.01 and 2.81 ± 0.01, representing an increase of 376% and 384% of
404 OD_{600} within the first 24 h of cultivation. In the meantime, SR8A6S3 achieved the growth of 584%
405 of initial cell concentration, achieving at 24 h of cultivation an OD_{600} of 3.90 ± 0.03. The *sor1*Δ
406 decreased the xylose consumption rate, while *gre3*Δ increased this rate at 24 h, but still lower than
407 SR8A6S3 (**Table 5**).
408

Table 5. Fermentation profiles of SR8A6S3-CDT_2-$GH43_{2/7}$, SR8A6S3-CDT_2, and SR8A6S3 under anaerobic conditions.

	At 24 h				At 72 h					
	r_{xylose}	r_{xylose}*	$P_{xylitol}$	$P_{Ethanol}$	r_{xylose}	r_{xylose}*	$P_{xylitol}$	$P_{Ethanol}$	$Y_{Ethanol}$	$Y_{Xylitol}$
SR8A6S3-CDT_2-$GH43_{2/7}$	0.54±0.03	0.15±0.01	0.00±0.00	0.77±0.05	0.57±0.01	0.10±0.00	0.01±0.00	0.45±0.00	0.47±0.01	0.018.±0.000
SR8A6S3-CDT_2	0.37±0.13	0.10±0.03	0.00±0.00	0.62±0.06	0.63±0.03	0.10±0.02	0.01±0.00	0.41±0.01	0.44±0.01	0.015.±0.001
SR8A6S3	0.94±0.06	0.19±0.01	0.00±0.00	0.74±0.00	0.83±0.02	0.14±0.00	0.03±0.00	0.47±0.00	0.42±0.00	0.032±0.0000

Parameters: r_{xylose}, xylose consumption rate (g L^{-1} h^{-1}); r_{xylose}*, specific xylose consumption rate (g L^{-1} OD^{-1} h^{-1}); $P_{xylitol}$, volumetric xylitol productivity (g L^{-1} h^{-1}); $P_{Ethanol}$, volumetric ethanol productivity (g L^{-1} h^{-1}); $Y_{Ethanol}$, ethanol yield (g $g_{consumed\ carbon\ source}^{-1}$); $Y_{Xylitol}$, xylitol yield (g $g_{consumed\ carbon\ source}^{-1}$).

Wenger et al. (2010) screened a large number of *S. cerevisiae* strains from wild, industrial, and laboratory backgrounds to determine the xylose-positive phenotype. Of 647 studied strains, some wine strains appeared to be able to grow modestly on xylose. By the application of high-throughput sequencing to bulk segregant analysis, they were able to identify a novel *XDH* gene homologous to *SOR1* (which was called *XDH1*) responsible for this phenotype. Next, the authors performed a comprehensive analysis of the involvement of the genes *GCY1, GRE3, YDL124W, YJR096W, YPR1, SOR1, SOR2, XDH1, XYL2,* and *XKS1* in the *XDH1* background strain (which has a xylose-positive phenotype) by single or combined deletion of the target genes. Single deletion of putative xylitol dehydrogenases (*SOR1*, *SOR2,* and *XYL2*) increased xylose utilization rate relative to the positive control; this phenotype was further enhanced when all three genes were deleted (*sor1*Δ *sor2*Δ *xyl2*Δ) (Wenger et al., 2010).

To assess the effect of endogenous xylitol-assimilating pathway genes on xylitol production profile by an engineered *S. cerevisiae* industrial strain CK17 overexpressing *Candida tropicalis XYL1* (encoding xylose reductase) in both batch and fed-batch fermentation with xylose and glucose as carbon sources, Yang et al. (2021) performed single deletion of the following genes: *XYL2* (yielding the strain CK17Δ*xyl2*), *SOR1*/*SOR2* (yielding the strain CK17Δ*sor*), and *XKS1* (yielding the strain CK17Δ*xks1*) (Yang et al., 2021). According to the authors, the mutant *sorΔ* had a reduced xylose consumption rate (12.4%) and xylitol production rate (4.7%), compared with its parental strain CK17, which is consistent with our findings for SR8A6S3-CDT_2. The strain CK17Δ*xks1* had the highest xylose consumption rate (0.65 g L^{-1} h^{-1}) and xylitol production rate (0.644 g L^{-1} h^{-1}), while the control strain consumed xylose and xylitol at 0.598 g L^{-1} h^{-1} and 0.549 g L^{-1} h^{-1} , respectively (Yang et al., 2021).

The *GRE3* gene was also deleted to improve xylose metabolism in *S. cerevisiae* CEN.PK2-1C expressing the xylose isomerase encoding gene *xylA* from *Thermus thermophilus*. The recombinant *gre3*Δ strains produced less xylitol than the parental strain (Träff et al., 2001). According to the authors, deletion of *GRE3* in *S. cerevisiae* decreased xylitol formation two- to threefold but not completely as xylitol may also be formed by the products of other genes, such as *XDH* (homologous to *SOR1* gene), through the reduction of xylulose or putative XR enzyme (Patiño et al., 2019; Richard et al., 1999; Wenger et al., 2010). Similarly, in the construction of a *S. cerevisiae* strain expressing the isomerase pathway (*xylA*) from the anaerobic fungus *Orpinomyces* sp. (GenBank No. MK335957), *gre3*Δ, *sor1*Δ, *XYL3,* and *TAL1* were added to reduce xylitol accumulation and increase the growth rate (Jeong et al., 2020).

On the other hand, overexpression of the endogenous genes *GRE3* and *XYL2*, coding for nonspecific aldose reductase and xylitol dehydrogenase, respectively, under endogenous

promoters, enhanced the growth of *S. cerevisiae* on xylose in the presence of glucose in aerobic shake flask cultivation (Toivari et al., 2004). However, significantly more xylitol was formed by the CEN.PK2 strain overexpressing the *S. cerevisiae* enzymes in comparison to the strain that carries *XR* and *XDH* from *S. stipitis*. Also, transcriptional analysis of xylose and glucose grown cultures shows that the expression of *SOR1*, which encodes sorbitol dehydrogenase, was elevated in transformed cultures. Thereby, the presence of xylose resulted in higher *XDH* activity and induced the expression of the *SOR1* gene which also has *XDH* activity (Toivari et al., 2004).

GRE3 and *SOR1* genes were considered for improving xylose fermentation based on these previous studies. In some of them, *sor1*Δ increased xylose utilization, and *gre3*Δ plus *sor1*Δ decreased xylitol accumulation. Similarly, we have observed that *gre3*Δ plus *sor1*Δ in *S. cerevisiae* SR8A6S3 decrease xylitol formation (**Table 5**). However, in contrast, *sor1*Δ alone did not increase the xylose consumption rate by SR8A6S3 (**Table 5**) as reported by (Wenger et al., 2010).

3.3. GH43 beta-xylosidases are intracellularly active

The activity of GH43-2 and GH43-7 in cell extracts of SR8A6S3 and SR8A6S3-CDT_2-$GH43_{2/7}$ was determined with pNPX as substrate (**Fig. 4**). No β-xylosidase activity was detected in the control strain, which is consistent with the absence of both genes *gh43-2* and *gh43-7* in its genome. On the other hand, the strain SR8A6S3-CDT_2-$GH43_{2/7}$ showed β-xylosidase activities of 27.74 U mL^{-1}, or 114.53 U g_{CDW}^{-1}, or 0.160 U $mg_{Protein}^{-1}$. The expression of both GH43-2 and GH43-7 is essential for converting XOS into xylose as the XR also acts as an XOS reductase, producing xylosyl-xylitol as a potential dead-end product, as first presented by Li et al., (2015). According to their work, despite the β-xylosidase GH43-7 having weak β-xylosidase activity, it rapidly cleaves xylosyl-xylitol into xylose and xylitol (Li et al., 2015).

473 Within the context of XOS-to-ethanol production, other fungal xylanases have also been
474 functionally expressed in *S. cerevisiae*, for example, β-xylosidase from *Aspergillus oryzae*
475 NiaD300 and xylanase II from *Trichoderma reesei* QM9414, which had activities in *S. cerevisiae*
476 MT8-1 of 234 U g_{CDW}^{-1} and 16 U g_{CDW}^{-1}, respectively (Katahira et al., 2004); β-xylosidase from
477 *T. reesei* QM9414 gave an activity of 6 nmol min^{-1} $mg_{Protein}^{-1}$ in *S. cerevisiae* M4-D4 (Fujii et al.,
478 2011); Sakamoto and co-authors (2012) expressed an endoxylanase (*T. reesei*) and a β-xylosidase
479 (*A. oryzae*) in *S. cerevisiae* MT8-1 and their activities were 41.2 U g_{CDW}^{-1} and 16.8 U g_{CDW}^{-1},
480 respectively (Sakamoto et al., 2012); and most recently, endoxylanase from *T. reesei* QM6a was
481 expressed in *S. cerevisiae* EBY100 giving activity of 1.197 U mg^{-1} (Tabañag et al., 2018).
482

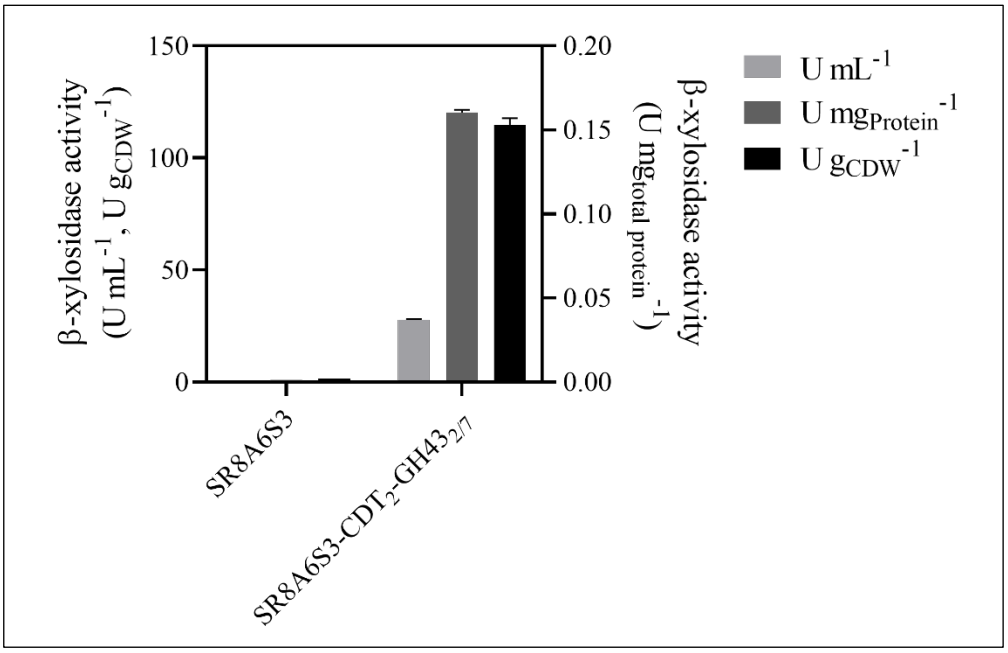

483

484 **Fig. 4.** Intracellular β-xylosidase activity of SR8A6S3 and SR8A6S3-CDT_2-$GH43_{2/7}$ pellet
485 extracts. The strains were cultured in YP-medium supplemented with 20 g L^{-1} glucose, 80 g L^{-1}
486 xylose, and 8 g L^{-1} acetate) under microaerobic conditions until the late log phase. The intracellular

487 GH43-2 and GH43-7 activities with pNPX as substrate were calculated relative to mg of protein
488 and g of cell dry weight.
489
490 **3.4. Fermentation of hydrolysed xylan by the engineered SR8A6S3-CDT$_2$-GH43$_{2/7}$ strain**
491 To evaluate XOS utilization, strain SR8A6S3-CDT$_2$-GH43$_{2/7}$ and the parental (control)
492 strain SR8A6S3 were cultivated under micro-aerobic conditions at 30 °C, in a YP medium
493 supplemented with hydrolysed xylan (YPXyl) and a mix of hydrolysed xylan plus acetate
494 (YPAXyl) media. These media were designed to mimic a hemicellulosic hydrolysate but without
495 the presence of inhibitory compounds, which can negatively influence yeast fermentations (Cola
496 et al., 2020; Kłosowski and Mikulski, 2021). The engineered strain and its parental strain were
497 cultivated in YPXy (**Fig. 5B** and **5D**), and in YPAXyl (**Fig. 5A** and **5C**) with an initial OD_{600} of
498 10 and, as expected, the engineered strain, SR8A6S3-CDT$_2$-GH43$_{2/7}$, produced higher titers of
499 ethanol than the parental strain SR8A6S3 in all conditions tested.
500 Xylobiose (X2) and xylotriose (X3) were the main carbon sources available in the medium.
501 X2 concentrations decreased during the growth of both strains, SR8A6S3-CDT$_2$-GH43$_{2/7,}$ and
502 SR8A6S3 (**Fig. 5**), although SR8A6S3 did not express either heterologous xylanolytic enzymes
503 or an XOS-transporter. One explanation could be that X2 entered the cell through a natural
504 transport system in *S. cerevisiae* and was converted into the non-metabolizable compound xylosyl-
505 xylitol by XR (xylose reductase), as observed previously by Li and colleagues (Li et al., 2015). It
506 is important to note that *S. cerevisiae* can consume disaccharides such as maltose, sucrose, and
507 trehalose, which are up taken through the action of membrane transporters (Lagunas, 1993). The
508 uptake of sucrose (disaccharide composed of glucose and fructose) can occur via the proton-
509 symport (*Mal11p*) (Marques et al., 2018). While trehalose (disaccharide composed of two glucose)

510 can be taken up via Agt1p-mediated trehalose transport followed by intracellular hydrolysis
511 catalysed by trehalase *Nth1*. Further, *AGT1*/*MAL11* gene is controlled by the *MAL* system. Maltose
512 is transported to the cytosol by an energy-dependent process coupled to the electrochemical proton
513 gradient (Lagunas, 1993).
514

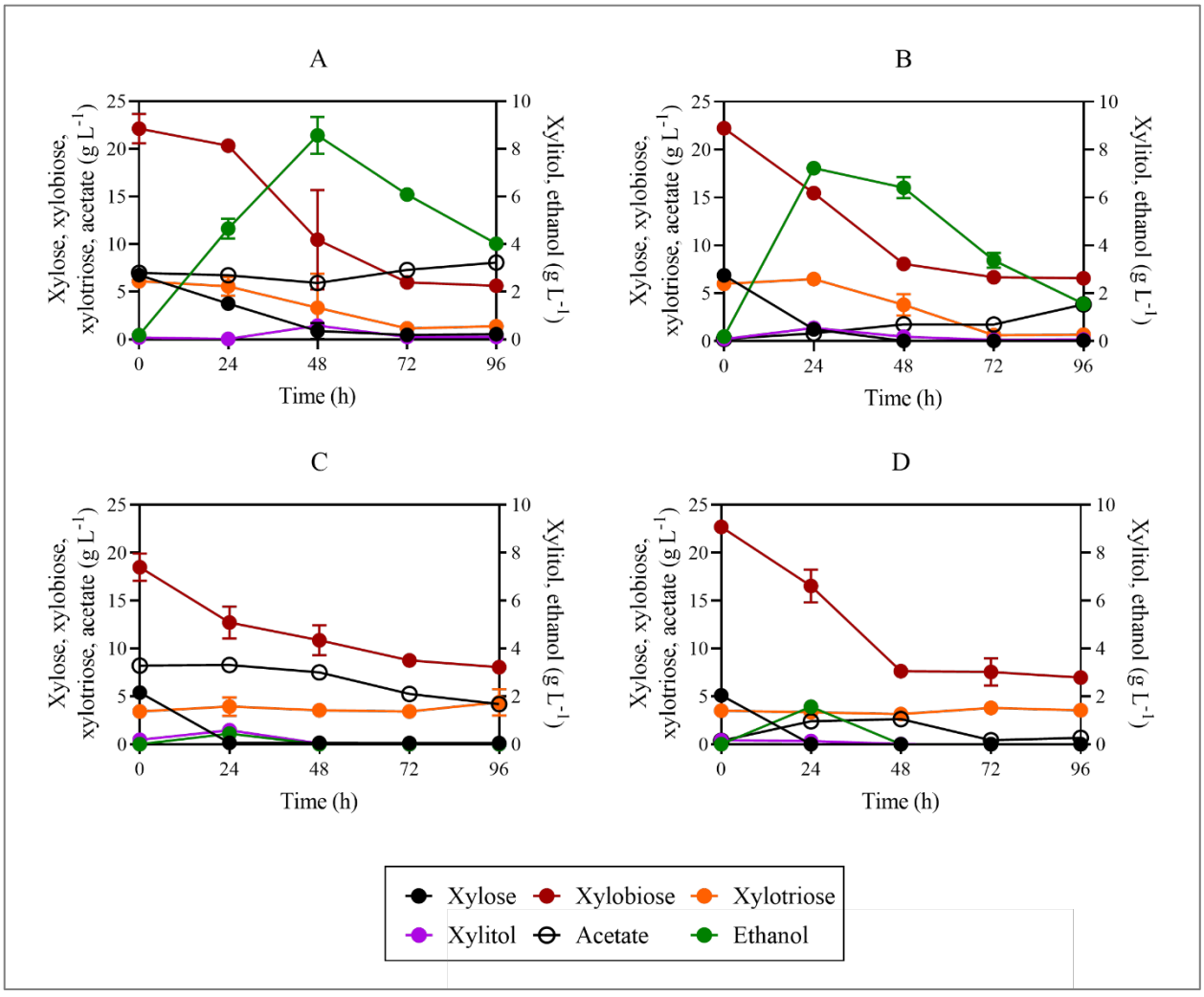

515

516 **Fig. 5**. Fermentation profiles of SR8A6S3-CDT$_2$-GH43$_{2/7}$ (A and B) and SR8A6S3 (C and D)
517 during batch cultivation in YPAXyl (YP medium containing hydrolysed xylan and acetate), A and
518 C, and YPXyl (YP medium containing hydrolysed xylan), B and D. Cultivations were performed

519 at 30 °C and 100 rpm with an initial OD_{600} of 10. Data are presented as the mean value and standard
520 deviation of two independent biological replicates.
521
522 Within the first 24 h of cultivation, SR8A6S3 depleted all xylose present in the medium
523 (**Fig. 5C** and **5D**) while SR8A6S3-CDT_2-$GH43_{2/7}$ spent more time fermenting xylose completely
524 (**Fig. 5A** and **5B**). At the same time, the doubly engineered strain consumed 6.77 ± 0.03 g L^{-1} of
525 X2, which represents 30% of the initial X2 concentration and 1.79 ± 1.08 g L^{-1} of X2 (8% of the
526 initial X2 concentration) respectively for the cultivations in YPXyl and YPAXyl. The presence of
527 acetate changed the X2 consumption profile by SR8A6S3-CDT_2-$GH43_{2/7}$ (**Fig. 5A**). Intriguingly,
528 the presence of X2 changed the acetate consumption profile by the parent strain, which consumed
529 4% of the initial acetate concentration until 24 h and 10% of the initial acetate concentration within
530 first 48 h of cultivation (**Fig. 5C**). The slight acetate reduction within 24 and 48 h of cultivation
531 might be affected by the oxidation of ethanol (Xu et al., 2022), which peak was at 24 h (**Fig. 5C**).
532 Concerning the X3 consumption profile, the parent strain SR8A6S3 barely metabolized X3 in
533 either medium (**Fig. 5C** and **5D**). Conversely, the engineered strain started to metabolize X3 after
534 24 h. The higher initial concentration of X2 than X3 probably interfered in X3 transportation.
535 Instead, in 24 – 48 h, SR8A6S3-CDT_2-$GH43_{2/7}$ consumed 2.67 ± 0.85 g L^{-1} and 1.73 ± 1.32 g L^{-1}
536 of X3 from YPXyl (**Fig. 5B**) and YPAXyl (**Fig. 5A**) cultivations, respectively. After 72 h of
537 cultivation, no substantial decrease in X3 amount was observed for XOS-consuming strain
538 cultivations.
539 The ethanol yield from SR8A6S3-CDT_2-$GH43_{2/7}$ was much higher than the control in both
540 media (**Table 6**). Furthermore, although in 96 h of cultivation both strains consumed
541 approximately the same amount of X2 in YPXyl (**Fig. 5B** and **5D**), only strain SR8A6S3-CDT_2-

542 $GH43_{2/7}$ appeared to ferment it to ethanol. Deletion of *gre3* and *sor1* delayed xylitol production
543 by SR8A6S3-CDT_2-$GH43_{2/7}$ strain. Interestingly, similar amounts of xylitol were observed for
544 both control and engineered strains when cultured in YPAXyl, 0.59 ± 0.00 g L^{-1} and 0.57 ± 0.10 g
545 L^{-1}, respectively. However, at 24 h of cultivation for SR8A6S3 and 48 h for SR8A6S3-CDT_2-
546 $GH43_{2/7}$.
547
548 **3.5.Fermentation of hemicellulosic hydrolysate by the engineered SR8A6S3-CDT_2-$GH43_{2/7}$**
549 **strain**
550 Following successful cultivation in a simulated hemicellulose hydrolysate, strain
551 SR8A6S3-CDT_2-$GH43_{2/7}$ was cultivated under micro-aerobic conditions in a YP medium
552 supplemented with an authentic XOS-rich hemicellulosic hydrolysate (Brenelli et al., 2020) (**Fig.**
553 **6A** and **6B**), which mimics the context of a lignocellulosic biorefinery, which makes full use of
554 hemicellulose. The breakdown of hemicellulose, which is acetylated (Kłosowski and Mikulski,
555 2021) releases highly toxic acetate, reducing the fermentative performance of *S. cerevisiae*
556 (Bellissimi et al., 2009; Li et al., 2015). SR8A6S3 was previously engineered through an optimized
557 expression of *AADH* and *ACS* in the acetate reduction pathway, enabling acetate conversion into
558 ethanol by the optimized strain (Zhang et al., 2016). We, therefore, tested whether the acetate
559 reduction pathway could operate simultaneously with XOS fermentation, as a means to augment
560 ethanol yield from the lignocellulosic hydrolysate.
561 Under this condition, we observed that xylose, X2, and X3 presented similar consumption
562 profiles in the XOS-consuming strain cultivation. These carbon sources were primarily consumed
563 before 24 h of cultivation. The latest engineered strain consumed 6.57 ± 0.28 g L^{-1} of xylose, which
564 represents 92% of the initial xylose concentration, and 7.57 ± 0.08 g L^{-1} of X2, which represents

565 97% of the initial X2 concentration, and 2.76 ± 0.14 g L^{-1} of X3 (69% of the initial X3
566 concentration). Conversely, during the same period, the parent strain consumed only 3.73 ± 0.94
567 g L^{-1} of xylose (55% of the initial xylose concentration), and 16% and 15.5% of the initial X2 and
568 X3 concentrations, respectively. It is worth pointing out that, as abovementioned, SR8A6S3 did
569 not express either heterologous xylanolytic enzymes or an XOS-transporter, the uptake of XOS
570 probably occurs through the action of membrane transporters that carry out disaccharides transport.
571 Although we observed a decrease in X2 and X3 amounts in the cultivations with the control
572 strain, only in cultivations with the XOS-consuming strain (SR8A6S3-CDT_2-$GH43_{2/7}$) ethanol
573 accumulation was consistent with X2 fermentation, i.e., conversion of X2 into ethanol (**Fig. 6A**).
574 SR8A6S3-CDT_2-$GH34_{2/7}$ and SR8A6S3-CDT_2 achieved the highest ethanol concentration at 24 h
575 of cultivation, 3.78 ± 0.53 g L^{-1} and 1.23 ± 0.10 g L^{-1}, respectively. In other terms, the newest
576 engineered strain achieved an ethanol yield of 0.50 ± 0.03 g $g_{consumed\ xylose}^{-1}$ and for the control
577 strain ethanol yield was 0.33 ± 0.08 g $g_{consumed\ xylose}^{-1}$ (**Table 6**). Interestingly, the ethanol peach
578 did not follow xylose exhaustion in the control cultivation (**Fig. 6B**), as happened to the engineered
579 strain cultivation (**Fig. 6A**).
580 Acetate consumption was not observed in both SR8A6S3 and SR8A6S3-CDT_2-$GH34_{2/7}$
581 cultivations within the first 24 h of cultivation. These results might indicate that transportation of
582 X2 and X3 might result in changes of the balance of NADH / NAD^+ and ATP which impaired
583 acetate consumption profile. In a previous study, Zhang et al. (2016) highlighted that three major
584 factors might limit the metabolic fluxes of the acetate reduction pathway, which include the
585 intracellular ATP levels, NADH levels, and the activities of key enzymes (*ACS* and *AADH*), being
586 the last the major limiting factor among them. In this study, the expression of key enzymes was
587 not modified through genetic interventions. In 24 – 96 h of cultivation, acetate was reduced by

588 25% and 53% for the XOS-consuming and control strains, respectively. The acetate profile seems
589 to be a combination of acetate consumption and acetate production, resulting from ethanol
590 oxidation (Xu et al., 2022). The lesser change in acetate consumption profile for SR8A6S3-CDT$_2$-
591 GH34$_{2/7}$ than SR8A6S3 might have resulted from the higher amount of ethanol produced by this
592 strain, which could be converted into acetate after exhaustion of the sugars (Xu et al., 2022).
593 Hence, it appears to use less acetate. Regarding xylitol production, the SR8A6S3-CDT$_2$-GH43$_{2/7}$
594 strain produced a lower xylitol yield, 0.041 ± 0.01 g $g_{consumed\ xylose}^{-1}$, than the control cultivation, in
595 which the yield was 0.083 ± 0.01 g $g_{consumed\ xylose}^{-1}$.
596

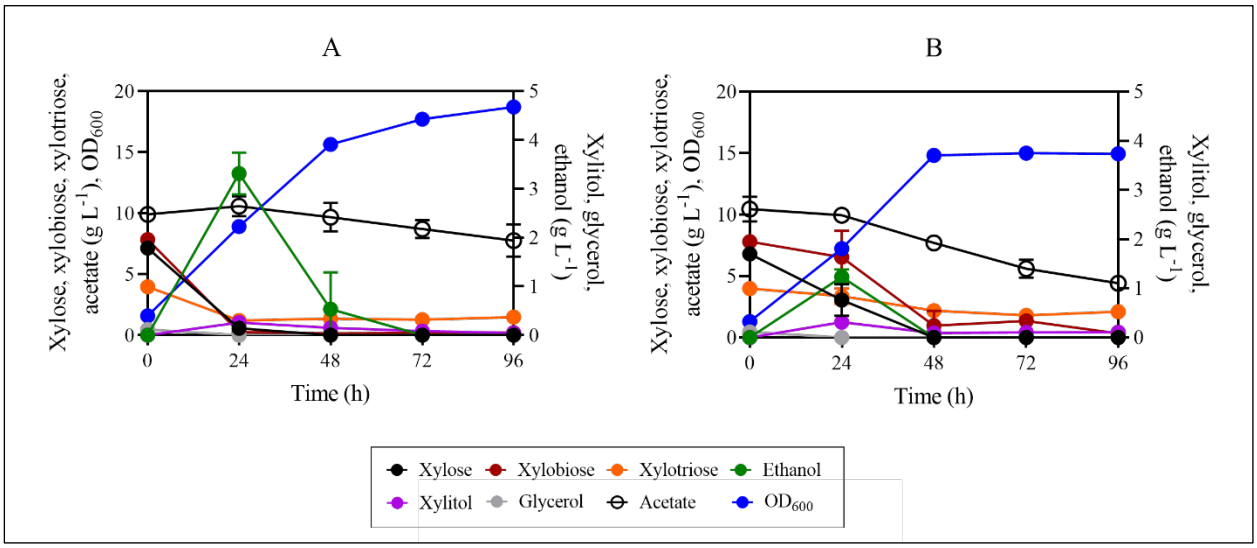

597

598 **Fig. 6**. Fermentation profiles of SR8A6S3-CDT$_2$-GH43$_{2/7}$ (A) and SR8A6S3 (B) during batch
599 cultivation in YPXAH (YP medium containing xylose, acetate, and hydrolysed hemicellulose).
600 Cultivations were performed at 30 °C and 100 rpm with an initial OD_{600} of 1. Data are presented
601 as mean values and standard deviations of two independent biological replicates.
602

603 To evaluate the improvement obtained by the introduction of the XOS-consumption
604 pathway in the SR8A6S3 strain, ethanol yield based on grams of consumed xylose was calculated

for each condition (**Table 6**). The ethanol yield of the SR8A6S3-CDT_2-$GH43_{2/7}$ strain increased substantially as compared to the SR8A6S3 strain. This substantial yield increase is very likely due to the conversion of XOS to ethanol.

Table 6. Ethanol yield of SR8A6S3-CDT_2 and SR8A6S3 under micro-aerobic cultivation at 30 °C, in YP medium, supplemented with a mix of hemicellulosic hydrolysed plus xylose and acetate (YPXAH), hydrolysed xylan (YPXyl) or a mix of hydrolysed xylan plus acetate (YPAXyl) with varied initial OD_{600}.

	Cultivation medium	Initial OD_{600}	$Y_{Ethanol}$
SR8A6S3-CDT_2-$GH43_{2/7}$	YPXAH	1	0.50 ± 0.03
	YPXAH	20	0.58 ± 0.08
	YPXyl	10	1.24 ± 0.04
	YPAXyl	10	1.43 ± 0.05
SR8A6S3	YPXAH	1	0.33 ± 0.08
	YPXyl	10	0.31 ± 0.00
	YPAXyl	10	0.08 ± 0.00

Parameters: $Y_{Ethanol}$, ethanol yield (g $g_{consumed\ xylose}^{-1}$).

Lignocellulose-derived ethanol provides environmental and economic benefits besides being a promising industry in the expected transition from fossil fuels to renewable energy (Kłosowski and Mikulski, 2021). Hemicellulosic-derived sugar comprises 15-35% of lignocellulosic biomass, representing a large source of renewable material that is available at a low cost (Dahlman et al., 2003; Gírio et al., 2010; Kłosowski and Mikulski, 2021). Engineered strains able to consume XOS derived from hemicellulose via intracellular hydrolysis represent a potential

benefit for bioethanol production since these strains would have a competitive advantage concerning other microorganisms, such as contaminating bacteria and wild *Saccharomyces* and non-*Saccharomyces* species that are expected to be unable to utilize XOS as a carbon source (Amorim et al., 2011; Procópio et al., 2022).

4. CONCLUSIONS

Xylose metabolism to ethanol in *S cerevisiae* SR8A6S3 is metabolically inefficient due to the production of xylitol. In this study we have integrated genes necessary to create a XOS-consumption pathway into two xylitol-production-related genes, *SOR1* and *GRE3*. The resulting strains, SR8A6S3-CDT_2 and SR8A6S3-CDT_2-$GH43_{2/7}$, which are *sor1*Δ and *sor1*Δ, *gre3*Δ, respectively, showed a reduction in xylitol production and improvement in ethanol yield when compared with their parental strain SR8A6S3 in YPDXA cultivations under both micro-aerobic and anaerobic conditions. However, this coincided with a reduced rate of xylose metabolism, implying that there is scope for improvement in overall flux from xylose to ethanol. SR8A6S3-CDT_2-$GH43_{2/7}$ was able to ferment X2 and X3 efficiently for ethanol production and achieved the highest apparent ethanol yield (based only on the content of monomeric xylose) of 1.43 ± 0.05 g $g_{consumed\ xylose}^{-1}$ (64% higher than theoretical ethanol yield) in YP supplemented with hydrolysed xylan and acetate. When grown on a medium containing hemicellulose hydrolysate with low monomeric xylose content, fermentation of X2 and X3 was poor, but this was dramatically improved by the addition of monomeric xylose. This, and other evidence which shows that X2 and X3 metabolism slows down once the monomeric carbohydrates have been depleted, suggests that the latter are required to provide the energy demands of the former (e.g. for enzyme biosynthesis). While there is clearly room for further improvement, this demonstrates that a XOS fraction

644 generated by simple hydrothermal/steam explosion pre-treatment of lignocellulosic agricultural
645 residues, without any subsequent enzymatic hydrolysis, is a potential resource for renewable
646 biofuel production using a XOS-utilising yeast.
647

648 ## 5. CREDIT AUTHORSHIP CONTRIBUTION STATEMENT

649 **Dielle P. Procópio:** Methodology, Investigation, Formal analysis, Data curation, Validation,
650 Writing – original draft, preparation. **Jae W. Lee:** Methodology. **Jonghyeok Shin:** Methodology.
651 **Robson Tramontina:** Methodology. **Fabio Squina:** Formal analysis **André Damasio:** Formal
652 analysis, Resources, Writing – review & editing. **Lívia P. Brenelli:** Methodology and Formal
653 analysis. **Sarita C. Rabelo:** Formal analysis. **Rosana Goldbeck:** Methodology and Formal
654 analysis. **Telma T. Franco:** Resources and Formal analysis. **David Leak**: Formal analysis,
655 Writing – review & editing. **Yong-Su Jin:** Supervision, Formal analysis, Project administration.
656 **Thiago O. Basso:** Supervision, Formal analysis, Resources, Project administration, Writing –
657 review & editing.
658

659 ## 6. ACKNOWLEDGMENT

660 We would like to thank The Brazilian Biorenewables National Laboratory
661 (LNBR/CNPEM/MCTIC) for infrastructure.
662

663 ## 7. FUNDING

664 This work was supported by the São Paulo Research Foundation (FAPESP) [grants numbers
665 #2015/50590-4, #2015/50612-8, #2017/15477-8, #2018/17172-2, #2018/01759-4, #2019/18075-
666 3, and #2021/04254-3].

667

668 **8. REFERENCES**

669 Adsul, M., Sandhu, S.K., Singhania, R.R., Gupta, R., Puri, S.K., Mathur, A., 2020. Designing a
670 cellulolytic enzyme cocktail for the efficient and economical conversion of lignocellulosic
671 biomass to biofuels. Enzyme Microb. Technol. 133, 109442.
672 https://doi.org/10.1016/J.ENZMICTEC.2019.109442

673 Almeida, J.R.M., Modig, T., Petersson, A., Hähn-Hägerdal, B., Lidén, G., Gorwa-Grauslund,
674 M.F., 2007. Increased tolerance and conversion of inhibitors in lignocellulosic hydrolysates
675 by *Saccharomyces cerevisiae*. J. Chem. Technol. Biotechnol. 82, 340–349.
676 https://doi.org/10.1002/jctb.1676

677 Amorim, H. V., Lopes, M.L., de Castro Oliveira, J.V., Buckeridge, M.S., Goldman, G.H., 2011.
678 Scientific challenges of bioethanol production in Brazil. Appl. Microbiol. Biotechnol. 91,
679 1267–1275. https://doi.org/10.1007/s00253-011-3437-6

680 Ask, M., Bettiga, M., Mapelli, V., Olsson, L., 2013. The influence of HMF and furfural on redox-
681 balance and energy-state of xylose-utilizing *Saccharomyces cerevisiae*. Biotechnol. Biofuels
682 6, 22. https://doi.org/10.1186/1754-6834-6-22

683 Ávila, P.F., Martins, M., de Almeida Costa, F.A., Goldbeck, R., 2020. Xylooligosaccharides
684 production by commercial enzyme mixture from agricultural wastes and their prebiotic and
685 antioxidant potential. Bioact. Carbohydrates Diet. Fibre 24, 100234.
686 https://doi.org/10.1016/J.BCDF.2020.100234

687 Bellissimi, E., van Dijken, J.P., Pronk, J.T., van Maris, A.J.A., 2009. Effects of acetic acid on the
688 kinetics of xylose fermentation by an engineered, xylose-isomerase-based *Saccharomyces*
689 *cerevisiae* strain. FEMS Yeast Res. 9, 358–364. https://doi.org/10.1111/j.1567-

690 1364.2009.00487.x

691 Bradford, M.M., 1976. A rapid and sensitive method for the quantitation of microgram quantities
692 of protein utilizing the principle of protein-dye binding. Anal. Biochem. 72, 248–254.
693 https://doi.org/10.1016/0003-2697(76)90527-3

694 Brenelli, L.B., Figueiredo, F.L., Damasio, A., Franco, T.T., Rabelo, S.C., 2020. An integrated
695 approach to obtain xylo-oligosaccharides from sugarcane straw: From lab to pilot scale.
696 Bioresour. Technol. 313, 123637. https://doi.org/10.1016/J.BIORTECH.2020.123637

697 Chen, C.-H., Yao, J.-Y., Yang-Barbara, Lee, H.-L., Yuan, S.-F., Hsieh, H.-Y., Liang, P.-H., 2019.
698 Engineer multi-functional cellulase/xylanase/β-glucosidase with improved efficacy to
699 degrade rice straw. Bioresour. Technol. Reports 5, 170–177.
700 https://doi.org/10.1016/j.biteb.2019.01.008

701 Chundawat, S.P.S., Beckham, G.T., Himmel, M.E., Dale, B.E., 2011. Deconstruction of
702 lignocellulosic biomass to fuels and chemicals. Annu. Rev. Chem. Biomol. Eng. 2, 121–145.
703 https://doi.org/10.1146/annurev-chembioeng-061010-114205

704 Cola, P., Procópio, D.P., Alves, A.T. de C., Carnevalli, L.R., Sampaio, I.V., da Costa, B.L., Basso,
705 T.O., 2020. Differential effects of major inhibitory compounds from sugarcane-based
706 lignocellulosic hydrolysates on the physiology of yeast strains and lactic acid bacteria.
707 Biotechnol. Lett. 42, 571–582. https://doi.org/10.1007/s10529-020-02803-6

708 Dahlman, O., Jacobs, A., Sjoè, J., 2003. Molecular properties of hemicelluloses located in the
709 surface and inner layers of hardwood and softwood pulps. Cellulose 10, 325–334.

710 Fujii, T., Yu, G., Matsushika, A., Kurita, A., Yano, S., Murakami, K., Sawayama, S., 2011. Ethanol
711 production from xylo-oligosaccharides by xylose-fermenting *Saccharomyces cerevisiae*
712 expressing β-xylosidase. Biosci. Biotechnol. Biochem. 75, 1140–6.

713 Gietz, R.D., Schiestl, R.H., Willems, A.R., Woods, R.A., 1995. Studies on the transformation of
714 intact yeast cells by the LiAc/SS-DNA/PEG procedure. Yeast 11, 355–360.
715 https://doi.org/10.1002/yea.320110408
716 Gírio, F.M., Fonseca, C., Carvalheiro, F., Duarte, L.C., Marques, S., Bogel-Łukasik, R., 2010.
717 Hemicelluloses for fuel ethanol: A review. Bioresour. Technol. 101, 4775–4800.
718 https://doi.org/10.1016/j.biortech.2010.01.088
719 Himmel, M.E., Ding, S.-Y.S.-Y., Johnson, D.K., Adney, W.S., Nimlos, M.R., Brady, J.W., Foust,
720 T.D., 2007. Biomass recalcitrance: Engineering plants and enzymes for biofuels production.
721 Science 315, 804–807. https://doi.org/10.1126/science.1137016
722 Jain, V.K., Divol, B., Prior, B.A., Bauer, F.F., 2011. Elimination of glycerol and replacement with
723 alternative products in ethanol fermentation by *Saccharomyces cerevisiae*. J. of Ind.
724 Microbiol. Biotechnol. 38, 1427–1435. https://doi.org/10.1007/s10295-010-0928-x
725 Jeong, D., Oh, E.J., Ko, J.K., Nam, J.-O., Park, H.-S., Jin, Y.-S., Lee, E.J., Kim, S.R., 2020.
726 Metabolic engineering considerations for the heterologous expression of xylose-catabolic
727 pathways in *Saccharomyces cerevisiae*. PLoS One 15, 1–18.
728 https://doi.org/10.1371/journal.pone.0236294
729 Karp, S.G., Medina, J.D.C., Letti, L.A.J., Woiciechowski, A.L., de Carvalho, J.C., Schmitt, C.C.,
730 de Oliveira Penha, R., Kumlehn, G.S., Soccol, C.R., 2021. Bioeconomy and biofuels: the case
731 of sugarcane ethanol in Brazil. Biofuels, Bioprod. Biorefining 15, 899–912.
732 https://doi.org/10.1002/BBB.2195
733 Katahira, S., Fujita, Y., Mizuike, A., Fukuda, H., Kondo, A., 2004. Construction of a xylan-
734 fermenting yeast strain through codisplay of xylanolytic enzymes on the surface of xylose-
735 utilizing *Saccharomyces cerevisiae* cells. Appl. Environ. Microbiol. 70, 5407–5414.

https://doi.org/10.1128/AEM.70.9.5407-5414.2004

Kim, H., Lee, W.H., Galazka, J.M., Cate, J.H.D., Jin, Y.S., 2014. Analysis of cellodextrin transporters from Neurospora crassa in *Saccharomyces cerevisiae* for cellobiose fermentation. Appl. Microbiol. Biotechnol. 98, 1087–1095. https://doi.org/10.1007/S00253-013-5339-2

Kim, S.R., Skerker, J.M., Kang, W., Lesmana, A., Wei, N., Arkin, A.P., Jin, Y.-S., 2013. Rational and evolutionary engineering approaches uncover a small set of genetic changes efficient for rapid xylose fermentation in *Saccharomyces cerevisiae*. PLoS One 8, 1–13. https://doi.org/10.1371/journal.pone.0057048

Klinke, H.B., Thomsen, A.B., Ahring, B.K., 2004. Inhibition of ethanol-producing yeast and bacteria by degradation products produced during pre-treatment of biomass. Appl. Microbiol. Biotechnol. 66, 10–26. https://doi.org/10.1007/s00253-004-1642-2

Kłosowski, G., Mikulski, D., 2021. Impact of Lignocellulose Pretreatment By-Products on *Saccharomyces cerevisiae* strain ethanol red metabolism during aerobic and anaerobic growth. Mol. 2021, Vol. 26, Page 806 26, 806. https://doi.org/10.3390/MOLECULES26040806

Ko, J.K., Lee, S.M., 2018. Advances in cellulosic conversion to fuels: engineering yeasts for cellulosic bioethanol and biodiesel production. Curr. Opin. Biotechnol. https://doi.org/10.1016/j.copbio.2017.11.007

Kostylev, M., Otwell, A.E., Richardson, R.E., Suzuki, Y., 2015. Cloning should be simple: *Escherichia coli* DH5α-mediated assembly of multiple DNA fragments with short end homologies. PLoS One 10, e0137466. https://doi.org/10.1371/JOURNAL.PONE.0137466

Lagunas, R., 1993. Sugar transport in *Saccharomyces cerevisiae*. FEMS Microbiol. Rev. 10, 229–

242. https://doi.org/10.1111/J.1574-6968.1993.TB05869.X

Li, X., Chen, Y., Nielsen, J., 2019. Harnessing xylose pathways for biofuels production. Curr. Opin. Biotechnol. 57, 56–65. https://doi.org/10.1016/j.copbio.2019.01.006

Li, X., Yu, V.Y., Lin, Y., Chomvong, K., Estrela, R., Park, A., Liang, J.M., Znameroski, E.A., Feehan, J., Kim, S.R., Jin, Y.S., Louise Glass, N., Cate, J.H.D., 2015. Expanding xylose metabolism in yeast for plant cell wall conversion to biofuels. Elife 4, 1–16. https://doi.org/10.7554/eLife.05896

Liu, J.J., Kong, I.I., Zhang, G.C., Jayakody, L.N., Kim, H., Xia, P.F., Kwak, S., Sung, B.H., Sohn, J.H., Walukiewicz, H.E., Rao, C. V., Jin, Y.S., 2016. Metabolic engineering of probiotic *Saccharomyces boulardii*. Appl. Environ. Microbiol. 82, 2280–2287. https://doi.org/10.1128/AEM.00057-16

Marques, W.L., Mans, R., Henderson, R.K., Marella, E.R., Horst, J. ter, Hulster, E. de, Poolman, B., Daran, J.M., Pronk, J.T., Gombert, A.K., van Maris, A.J.A., 2018. Combined engineering of disaccharide transport and phosphorolysis for enhanced ATP yield from sucrose fermentation in *Saccharomyces cerevisiae*. Metab. Eng. 45, 121–133. https://doi.org/10.1016/J.YMBEN.2017.11.012

Mewis, K., Lenfant, N., Lombard, V., Henrissat, B., 2016. Dividing the large glycoside hydrolase family 43 into subfamilies: a motivation for detailed enzyme characterization. Appl. Environ. Microbiol. 82, 1686–1692. https://doi.org/10.1128/AEM.03453-15

Patiño, M.A., Ortiz, J.P., Velásquez, M., Stambuk, B.U., 2019. D-Xylose consumption by nonrecombinant *Saccharomyces cerevisiae*: A review. Yeast 36, 1–16. https://doi.org/10.1002/yea.3429

Procópio, D.P., Kendrick, E., Goldbeck, R., Damasio, A.R. de L., Franco, T.T., Leak, D.J., Jin,

782 Y.-S., Basso, T.O., 2022. Xylo-Oligosaccharide utilization by engineered *Saccharomyces*
783 *cerevisiae* to produce ethanol. Front. Bioeng. Biotechnol. 10, 1–21.
784 https://doi.org/10.3389/FBIOE.2022.825981/PDF
785 Queiroz, S.S., Jofre, F.M., Mussatto, S.I., Felipe, M. das G.A., 2022. Scaling up xylitol
786 bioproduction: Challenges to achieve a profitable bioprocess. Renew. Sustain. Energy Rev.
787 154, 111789. https://doi.org/10.1016/J.RSER.2021.111789
788 Raj, T., Chandrasekhar, K., Naresh Kumar, A., Rajesh Banu, J., Yoon, J.J., Kant Bhatia, S., Yang,
789 Y.H., Varjani, S., Kim, S.H., 2022. Recent advances in commercial biorefineries for
790 lignocellulosic ethanol production: Current status, challenges and future perspectives.
791 Bioresour. Technol. 344, 126292. https://doi.org/10.1016/J.BIORTECH.2021.126292
792 Raud, M., Kikas, T., Sippula, O., Shurpali, N.J., 2019. Potentials and challenges in lignocellulosic
793 biofuel production technology. Renew. Sustain. Energy Rev. 111, 44–56.
794 https://doi.org/10.1016/J.RSER.2019.05.020
795 Richard, P., Toivari, M.H., Penttilä, M., 1999. Evidence that the gene YLR070c of *Saccharomyces*
796 *cerevisiae* encodes a xylitol dehydrogenase. FEBS Lett. 457, 135–138.
797 https://doi.org/10.1016/S0014-5793(99)01016-9
798 Sakamoto, T., Hasunuma, T., Hori, Y., Yamada, R., Kondo, A., 2012. Direct ethanol production
799 from hemicellulosic materials of rice straw by use of an engineered yeast strain codisplaying
800 three types of hemicellulolytic enzymes on the surface of xylose-utilizing *Saccharomyces*
801 *cerevisiae* cells. J. Biotechnol. 158, 203–210.
802 https://doi.org/doi:10.1016/j.jbiotec.2011.06.025
803 Salas-Navarrete, P.C., de Oca Miranda, A.I.M., Martínez, A., Caspeta, L., 2022. Evolutionary and
804 reverse engineering to increase *Saccharomyces cerevisiae* tolerance to acetic acid, acidic pH,

805 and high temperature. Appl. Microbiol. Biotechnol. 106, 383–399.
806 https://doi.org/10.1007/S00253-021-11730-Z/FIGURES/9
807 Sarkar, N., Ghosh, S.K., Bannerjee, S., Aikat, K., 2012. Bioethanol production from agricultural
808 wastes: An overview. Renew. Energy 37, 19–27.
809 https://doi.org/10.1016/J.RENENE.2011.06.045
810 Sharma, B., Larroche, C., Dussap, C.G., 2020. Comprehensive assessment of 2G bioethanol
811 production. Bioresour. Technol. 313, 123630.
812 https://doi.org/10.1016/J.BIORTECH.2020.123630
813 Stovicek, V., Borodina, I., Forster, J., 2015. CRISPR–Cas system enables fast and simple genome
814 editing of industrial *Saccharomyces cerevisiae* strains. Metab. Eng. Commun. 2, 13–22.
815 https://doi.org/10.1016/J.METENO.2015.03.001
816 Sun, L., 2020. Engineering yeast to synthesize high-value natural products from plant cell wall.
817 University of Illinois at Urbana-Champaign.
818 Sun, L., Wu, B., Zhang, Z., Yan, J., Liu, P., Song, C., Shabbir, S., Zhu, Q., Yang, S., Peng, N., He,
819 M., Tan, F., 2021. Cellulosic ethanol production by consortia of *Scheffersomyces stipitis* and
820 engineered *Zymomonas mobilis*. Biotechnol. Biofuels 14, 1–13.
821 https://doi.org/10.1186/S13068-021-02069-8/FIGURES/5
822 Tabañag, I.D.F., Chu, I.M., Wei, Y.H., Tsai, S.L., 2018. Ethanol production from hemicellulose
823 by a consortium of different genetically-modified *Saccharomyces cerevisiae*. J. Taiwan Inst.
824 Chem. Eng. 89, 15–25. https://doi.org/10.1016/j.jtice.2018.04.029
825 Toivari, M.H., Salusjärvi, L., Ruohonen, L., Penttilä, M., 2004. Endogenous xylose pathway in
826 *Saccharomyces cerevisiae*. Appl. Environ. Microbiol. 70, 3681–3686.
827 https://doi.org/10.1128/AEM.70.6.3681-3686.2004

828 Träff, K.L., Cordero, R.R.O., Van Zyl, W.H., Hahn-Hägerdal, B., 2001. Deletion of the GRE3
829 aldose reductase gene and its influence on xylose metabolism in recombinant strains of
830 *Saccharomyces cerevisiae* expressing the *xylA* and *XKS1* genes. Appl. Environ. Microbiol.
831 67, 5668–5674. https://doi.org/10.1128/AEM.67.12.5668-5674.2001
832 Tramontina, R., Brenelli, L.B., Sodré, V., Franco Cairo, J.P., Travália, B.M., Egawa, V.Y.,
833 Goldbeck, R., Squina, F.M., 2020. Enzymatic removal of inhibitory compounds from
834 lignocellulosic hydrolysates for biomass to bioproducts applications. World J. Microbiol.
835 Biotechnol. 36, 1–11. https://doi.org/10.1007/S11274-020-02942-Y/TABLES/1
836 Tramontina, R., Robl, D., Maitan-Alfenas, G.P., de Vries, R.P., 2016. Cooperation of *Aspergillus*
837 *nidulans* enzymes increases plant polysaccharide saccharification. Biotechnol. J. 11, 988–
838 992. https://doi.org/10.1002/BIOT.201500116
839 Wei, N., Quarterman, J., Kim, S.R., Cate, J.H.D., Jin, Y.-S., 2013. Enhanced biofuel production
840 through coupled acetic acid and xylose consumption by engineered yeast. Nat. Commun. 4,
841 1–8. https://doi.org/10.1038/ncomms3580
842 Wenger, J.W., Schwartz, K., Sherlock, G., 2010. Bulk segregant analysis by high-throughput
843 sequencing reveals a novel xylose utilization gene from *Saccharomyces cerevisiae*. PLoS
844 Genet. 6, e1000942. https://doi.org/10.1371/journal.pgen.1000942
845 Xu, Z., Lin, L., Chen, Z., Wang, K., Sun, J., Zhu, T., 2022. The same genetic regulation strategy
846 produces inconsistent effects in different *Saccharomyces cerevisiae* strains for 2-
847 phenylethanol production. Appl. Microbiol. Biotechnol. 106, 4041–4052.
848 https://doi.org/10.1007/S00253-022-11993-0/FIGURES/7
849 Yang, B.X., Xie, C.Y., Xia, Z.Y., Wu, Y.J., Gou, M., Tang, Y.Q., 2021. Improving xylitol yield
850 by deletion of endogenous xylitol-assimilating genes: a study of industrial *Saccharomyces*

cerevisiae in fermentation of glucose and xylose. FEMS Yeast Res. 20. https://doi.org/10.1093/FEMSYR/FOAA061

Zhang, G.C., Kong, I.I., Wei, N., Peng, D., Turner, T.L., Sung, B.H., Sohn, J.H., Jin, Y.S., 2016. Optimization of an acetate reduction pathway for producing cellulosic ethanol by engineered yeast. Biotechnol. Bioeng. 113, 2587–2596. https://doi.org/10.1002/bit.26021